Renewable Energy 182 (2022) 923–933

Contents lists available at ScienceDirect

Renewable Energy

journal homepage: www.elsevier.com/locate/renene

An analytical model to evaluate the fatigue crack effects on the hybrid photovoltaic-thermoelectric device

Y.J. Cui [a], B.L. Wang [a, *], K.F. Wang [a], G.G. Wang [a, **], A.B. Zhang [b]

[a] Graduate School at Shenzhen, Harbin Institute of Technology, Harbin, 150001, PR China
[b] Piezoelectric Device Laboratory, School of Mechanical Engineering & Mechanics, Ningbo University, Ningbo, 315211, PR China

ARTICLE INFO

Article history:
Received 14 July 2021
Received in revised form
18 October 2021
Accepted 26 October 2021
Available online 29 October 2021

Keywords:
Thermoelectric material
Photovoltaic cell
Electric power output
Crack growth

ABSTRACT

A hybrid photovoltaic and thermoelectric device can effectively increase utilization of solar systems. In this article, an analytical model to evaluate the fatigue cracking and its effect on electric power of a hybrid photovoltaic-thermoelectric device is proposed. Both the analytical and simplified expressions of crack length and electric power versus the cyclic number are presented. It is found that combining thermoelectric module with photovoltaic cell of a small temperature coefficient 0.001 K^{-1} can improve the total electric power by 7.8%. Inclusion of thermoelectric module with photovoltaic cell of a large temperature coefficient 0.004 K^{-1} reduces the total electric power by 3.3%. The electric power of the hybrid device is inversely proportional to the cyclic number. For photovoltaic cells with small temperature coefficient, the total electric power decreases with crack propagation. The total electric power increases with crack propagation for photovoltaic cells of large temperature coefficient. The thickness ratio of photovoltaic cell to the insulating layer is optimized to eliminate the interlaminar shear stress thus greatly enhance lifetime. Lifetime of the hybrid devices can be availably improved by appropriately increasing thickness of the insulating layer. The optimized length of thermoelectric module for obtaining the maximum electric power output is given.

1. Introduction

Energy is always a significant issue for daily life and social development. The surrounding environment exists amount of energy including vibration, heat, wind, especially solar energy those can be harvested and converted into electric power [1,2]. Solar energy has numerous advantages including renewable, easily accessible, abundant, free and clean [3]. The solar radiation falling on the earth's surface every year is about 3400000 EJ, a value that is 7500 times higher than the total energy consumption of the whole world [4]. Additionally, the solar energy can be easily harvested and converted into electric energy through photovoltaic (PV) technology. Thus, research on photovoltaic cells has attracted great attention from both academia and industry [5]. In the process of solar energy converting into electricity, a large fraction of the solar radiation is degraded and released as heat. However, the PV performances of the commercial photovoltaic cells generally decrease with temperature [6]. Fortunately, the solid-state TE generators have the ability in directly converting the unwanted heat in the photovoltaic cells into electricity [7]. Thus, the hybrid PV-TE devices are naturally proposed to enhance the total energy conversion performance.

The TE module in the hybrid devices plays a two-fold manner: passively cooling down the photovoltaic cell and converting the unnecessary heat accumulating in the photovoltaic cells into electricity [8,9]. Therefore, the total electric power output of the hybrid device is greatly improved with comparison to the TE module and the photovoltaic cell working alone. For instance, it is observed that efficiency and the electric power for a monocrystalline PV cell working alone can be respectively improved 0.59% and 5.06% by integrating with the TE module [10]. In practical applications, a concentrator is commonly employed to enhance solar radiation. For the commercially used photovoltaic cells, it was found that the polycrystalline and amorphous silicon thin-films were suitable for forming the concentrated hybrid PV-TE devices, and the polymer photovoltaic cells were more appropriate for assembling the non-concentrated hybrid devices [11,12].

* Corresponding author.
** Corresponding author.
E-mail addresses: wangbl2001@hotmail.com, wangbl@hit.edu.cn (B.L. Wang), wangguigen@hit.edu.cn (G.G. Wang).

https://doi.org/10.1016/j.renene.2021.10.076
0960-1481/

Nomenclature

A	Cross-sectional area [m^2]
a	Length of fatigue crack [m]
C	Geometric concentration factor
E	Young's modulus [GPa]
F	axial force [N]
G	Solar radiance [W/m^2]
H	Thickness [m]
I	Electric current [A]
K	Stress intensity factor [Pa m$^{1/2}$]
k	Thermal conductivity [W/(m•K)]
L	Length of TE leg [m]
N_F	Fatigue life
P	Power output [W]
q_{in}	Incident heat flux [W/m^2]
q_1	Heat flux inputs into TE module [W]
q_0	Heat flux outputs from TE module [W]
R	Electric resistance [Ω]
s	Seebeck coefficient [V/K]
T_{pv}	Temperature of solar cell [K]
T_1	Temperature at hot side of TE module [K]
T_0	Temperature at cold side of TE module [K]

Greek letters

α	Coefficient of thermal expansion [1/K]
β_{ref}	Temperature coefficient of solar cell [1/K]
γ	Thermal conductance of TE module [W/K]
ε	Strain
η	Energy conversion efficiency
κ	Thermal resistance [K/W]
λ	Absorptivity of the solar cell
υ	Poisson's ratio
ρ	Electrical resistivity [Ω•m]
τ	Interlaminar shear stress [GPa]
ψ	Coefficient of axial compliance of equivalent solar cell [m/N]

Subscripts

c	Cooper strip
n	N-type thermoelectric leg
p	P-type thermoelectric leg
pv	Solar cell
ref	Reference performance at 298.15 K
TE	Thermoelectric module
t	Electric insulation layer

To further understand the characteristics and improve performance of the hybrid devices, numerous researches have been carried out. For example, feasibility of the hybrid devices was numerically analyzed [13]. The geometric configuration and thermoelectric figure-of-merit were optimized to generate a larger electric power output for the hybrid devices [14,15]. Additionally, effect of the cooling system in the hybrid devices on performance was also studied. For the hybrid PV-TE devices with a cooling system (heat pipe), it was reported that efficiency was 1.47% higher with comparison to that without cooling systems at a concentration ratio of 6 [16]. When the solar radiation was 5000 W/m^2 and the flow rate of coolant in the heat sink was 80 g/min, it was reported that the electric power of a hybrid device sandwiched by a micro-channel heat sink can reach 440 W/m^2, a value 1.2 times bigger than that without a heat sink [17]. Considering the hybrid PV-TE devices have more contact interfaces than the TE modules and the photovoltaic cells working alone, effect of the thermal resistances on performance was also analyzed. It was found that the electric power of the photovoltaic cells and the TE modules were improved at least 14% and 60% due to the decreasing thermal contact resistances [18]. The hybrid PV-TE devices even lost its superiority of improving the total electric power output if the thermal resistances were very huge. For example, efficiency of the hybrid devices and the reproductive photovoltaic cells working alone was 16.5% and 17.2% at the thermal contact resistance of 500 Kmm^2/W [19]. It was also found that the electric power of the photovoltaic cells and the TE modules in the hybrid devices could respectively improve 14% and 60% [20]. Therefore, it is very significant to reduce the thermal resistances to improve performance of the hybrid devices. All these contributions have developed of the hybrid PV-TE devices.

In the engineering applications, the high thermal loadings usually cause badly interlaminar stress in the composite structures [21,22]. It was found that there were abundant cracks in the TE module subjected to the thermal cyclic loadings, as shown in Fig. 1 [23]. It was reported that the thermoelectric figure-of-merit could reduce 20% through 40000 thermal cycles [24]. When the TE module subjected to a repeated thermal cycling from 30 °C to 160 °C, it was observed that the power output was approximately dropped 11% after 6000 cycles [25]. The sunlight impinging on the photovoltaic cells varies with time. Therefore, the hybrid PV-TE system under the cyclic thermal loadings will be destroyed by fatigue accumulation [26]. Physically, crack propagation weakens the ability of hybrid PV-TE system to transfer heat and conduct electricity, this certainly reduces the performance of the hybrid devices. However, characteristics of fatigue cracking and its influence on energy conversion performance of the hybrid devices are absent. Therefore, this paper firstly proposes a mathematical model to evaluate the fatigue cracking and its effect on electric power of the hybrid devices. Results obtained in this paper can provide a theoretical guideline for design, preparation and performance evaluation of the PV-TE devices. The computational code is developed in the mathematical programming environment Matlab. The data analysis and graphing are carried out in the software OriginPro. The details how to solve the mathematical model to obtain its fatigue life and electric power are presented in Sec. 3.

2. Energy conversion performance

Schematic diagram of a photovoltaic-thermoelectric (PV-TE) hybrid device is given in Fig. 2. The thermoelectric module can further convert the unnecessary heat in the photovoltaic cells into electricity and simultaneously cool the photovoltaic cells. To avoid the short circuit problem between the photovoltaic cells and the metal interconnectors (e.g. cooper strip), an insulating layer is deposited at the top surface of the interconnector. The TE module consists of the n- and p-type TE legs, sandwiched by an insulating layer whose thickness can be ignored. The TE legs and the interconnectors are assembled together using the silver paste as bonding agent. To analyze the effect of fatigue cracking on energy conversion performance, a through crack with length a is considered, as shown in Fig. 2. Without loss of generality, the heat flux and electric current are considered completely blocked at the crack region. Effects of crack on thermal transfer and electrical conduct are described, respectively, by thermal and electrical resistances.

Thickness of the n- and p-type TE legs are H_n and H_p. Length and

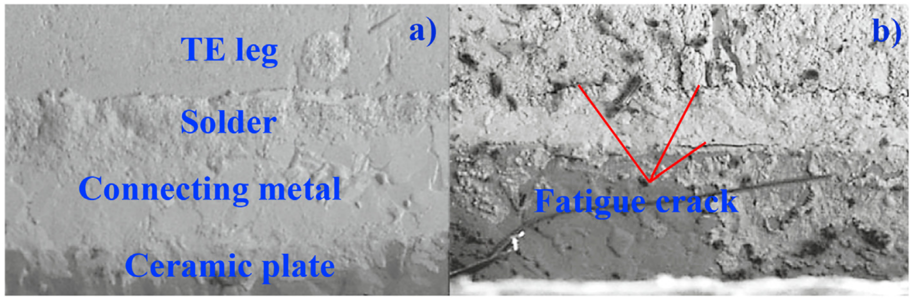

Fig. 1. The TE module before (a) and after (b) thermal cycling [23].

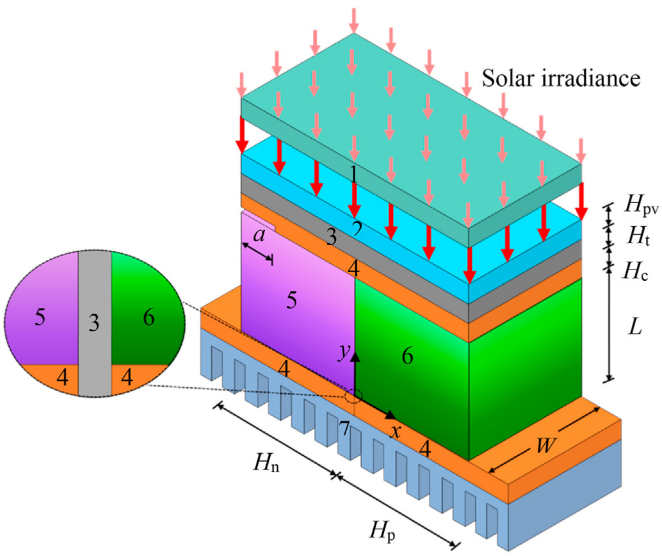

Fig. 2. Schematic diagram of the PV-TE devices. 1-solar concentrator, 2-photovoltic cell, 3-insulating layer, 4-metal interconnector, 5-n-type TE leg, 6-p-type TE leg, 7-heat sink.

width of the TE module are L and W. Thickness of the photovoltaic cell, the insulating layer and the metal interconnector are H_{pv}, H_t and H_c. When heat conduction in the hybrid device reaches the steady-state, temperature of the photovoltaic cell is T_{pv}, temperature at $y = L$ and $y = 0$ are T_1 and T_0. Additionally, it is assumed that: (1) The heat conduction is one-dimensional due to the thermal loading applying along the length direction. (2) Radiation and convection between the hybrid device and the ambient is neglected. (3) Thickness of the bonding agent (silver paste) is neglected except calculating the thermal resistance and electrical resistance.

It is reported that the incident heat flux impinging on the photovoltaic cell is [27] $q_{in} = \lambda CG$, in which λ is absorptivity, C denotes the geometric concentration factor and G represents the directly incident solar radiance. For a concrete working condition (the solar radiance G is determined), value of q_{in} can be treated as a constant. According to the principle of energy conservation, the electric power and efficiency of a photovoltaic cell is [14,15]:

$$P_{pv} = q_{in} A_{pv} \eta_{pv} \tag{1}$$

$$\eta_{pv} = \eta_{ref}\left[1 - \beta_{ref}\left(T_{pv} - T_{ref}\right)\right] \tag{2}$$

where A_{pv} is cross-sectional area of the photovoltaic cell, η_{ref} represents the reference efficiency measured at temperature $T_{ref} = 298.15$ K, β_{ref} denotes the corresponding temperature coefficient.

As shown in Eqs. (1) and (2), the electric power and efficiency of a photovoltaic cell are functions with respect to its temperature T_{pv}. The heat conduction law indicates that relationship between T_{pv} and T_1 holds [27]:

$$T_{pv} - T_1 = q_{in} A_{pv}(1 - \eta_{pv})\left(\kappa_{pv} + \kappa_t + A_{pv}\frac{\kappa_c + \kappa_s}{A_n + A_p}\right) \tag{3}$$

where A_n and A_p respectively denote cross-sectional areas of the n- and p-type TE legs, κ_{pv}, κ_t, κ_c and κ_s are thermal resistances of the photovoltaic cell, the insulating layer, the metal interconnector and silver paste defined as [27]: $\kappa_{pv} = H_{pv}/(k_{pv}A_{pv})$, $\kappa_t = H_t/(k_t A_{pv})$, $\kappa_c = H_c/(k_c A_{pv})$ and $\kappa_s = H_s/(k_s A_{pv})$, in which k_{pv}, k_e, k_c and k_s represent thermal conductivities of the photovoltaic cell, the insulating layer, the metal interconnector and silver paste, H_s is thickness of the silver paste.

The material properties (especially thermal conductivity, Seebeck coefficient and electrical resistivity) of the thermoelectric materials are sensitive to temperature [28]. Here, the temperature-dependent material properties of the TE mode are used. By using the heat conduction law again, the relationship between T_1 and T_0 holds [27]:

$$T_1 - T_0 = (1 - \eta_{pv})(1 - \eta_{TE})\frac{A_{pv}(1 - \omega)}{A_n + A_p}\frac{q_{in} L}{k_{ne} + k_{pe}} \tag{4}$$

where ω is a non-dimensional damage parameter defined as $\omega = a/H_n$, $\omega = 0$ means there is no crack, $\omega = 1$ indicates the whole TE leg is separated from the metal interconnector and the hybrid PV-TE device is crashed for this case, η_{TE} represents efficiency of the TE module, k_{ne} and k_{pe} are equivalent thermal conductivities given by Ref. [29]: $k_{ne} = \int_{T_0}^{T_1} k_n \mathrm{d}T/\Delta T$ and $k_{pe} = \int_{T_0}^{T_1} k_p \mathrm{d}T/\Delta T$, in which $\Delta T = T_1 - T_0$ denotes temperature drop across TE module, k_n and k_p are temperature-dependent thermal conductivities of TE legs. Similarly, the equivalent Seebeck coefficient and equivalent electrical resistivity are, respectively, defined as [29]: $s_{ie} = \int_{T_0}^{T_1} s_i \mathrm{d}T/\Delta T$ and $\rho_{ie} = \int_{T_0}^{T_1} \rho_i \mathrm{d}T/\Delta T$, (i='n','p').

From the perspective of energy conservation, the heat flux at $y = L$ is [30,31]:

$$q_1 = \gamma(1 - \omega)\Delta T + (s_{pe} + s_{ne})T_1 I - 0.5I^2 R_{TE} \tag{5}$$

and the heat flux at $y = 0$ is [30,31]:

$$q_0 = \gamma(1 - \omega)\Delta T + (s_{pe} - s_{ne})T_0 I + 0.5I^2 R_{TE} \tag{6}$$

where γ and R_{TE} are thermal resistance and internal electric resistances of the TE module, respectively defined as $\gamma = (k_{pe}A_p + k_{ne}A_n)/L$ and $R_{TE} = (\rho_{pe}/A_p + \rho_{ne}/A_n)L$, the electric current in the TE module is defined as [32] $I = (s_{pe} - s_{ne})\Delta T/(R_{TE} + R_L + R_{cont})$, in which R_L denotes the external electrical resistance, $R_{cont} = \rho_s H_s/[(A_n + A_p)(1 - \omega)]$ denotes the electrical contact resistance, ρ_s is the electrical resistivity of the silver paste.

Now, the electric power and efficiency of the TE module are:

$$P_{TE} = q_1 - q_0 = (s_{pe} - s_{ne})\Delta T I - I^2 R_{TE} \tag{7}$$

$$\eta_{TE} = \frac{P_{TE}}{q_1} = \frac{(s_{pe} - s_{ne})\Delta T I - I^2 R_{TE}}{\gamma(1-\omega)\Delta T + (s_{pe} - s_{ne})T_1 I - 0.5 I^2 R_{TE}} \tag{8}$$

As shown in Eq. (8), η_{TE} is a function versus T_1 and T_0. Generally, value of T_0 is known. This means value of η_{TE} is only determined by T_1. Additionally, Eqs. (2) and (3) clearly show that η_{pv} is also determined by T_1 for the concrete solar radiance. Thus, temperature of TE module at the hot side will be derived subsequently. Applying Eq. (3) into Eq. (2) gives:

$$\eta_{pv} = \eta_{ref} \frac{1 - \beta_{ref} q_{in} A_{pv}\left(\kappa_{pv} + \kappa_t + A_{pv}\frac{\kappa_c + \kappa_s}{A_n + A_p}\right) - \beta_{ref}\left(T_1 - T_{ref}\right)}{1 - \beta_{ref}\eta_{ref} q_{in} A_{pv}\left(\kappa_{pv} + \kappa_t + A_{pv}\frac{\kappa_c + \kappa_s}{A_n + A_p}\right)} \tag{9}$$

By substituting of Eqs. (8) and (9) into Eq. (4), one can obtain:

$$T_1 - T_0 = \frac{\eta_1 + \eta_{ref}\beta_{ref} T_1}{\eta_2} \frac{\gamma(1-\omega)\Delta T + (s_{pe} - s_{ne})T_0 I + 0.5 I^2 R_{TE}}{\gamma(1-\omega)\Delta T + (s_{pe} - s_{ne})T_1 I - 0.5 I^2 R_{TE}} \frac{A_{pv}(1-\omega)}{A_n + A_p} \frac{q_{in} L}{k_{ne} + k_{pe}} \tag{10}$$

together with

$$\eta_1 = 1 - \eta_{ref} - \eta_{ref}\beta_{ref} T_{ref} \tag{11}$$

$$\eta_2 = 1 - \beta_{ref}\eta_{ref} q_{in} A_{pv}\left(\kappa_{pv} + \kappa_t + A_{pv}\frac{\kappa_c + \kappa_s}{A_p + A_n}\right) \tag{12}$$

The solution of Eq. (10) in this paper is solved with a numerical method. The computational code can be programmed in the mathematical programming environment Matlab. By using Eq. (10), one can plot a curve Γ versus T_1 for a given value of the solar radiance q_{in}. The intersection point between Γ and the x-axis must be the root of Eq. (10). The electric power of the photovoltaic cell and the TE module can be directly solved by applying the known T_1 into Eqs. (1) and (7). Efficiency of the photovoltaic cell and the TE module can also be obtained by applying T_1 into Eqs. (9) and (8). Finally, the total electric power and efficiency of the hybrid device are $P_{PV\text{-}TE} = P_{pv} + P_{TE}$ and $\eta_{PV\text{-}TE} = P_{PV\text{-}TE}/(q_{in}A_{pv})$.

3. Fatigue cracking

Comparing to the length of thermoelectric (TE) legs, thickness of photovoltaic cell, insulating layer and metal interconnectors are small. Additionally, both insulating layer and interconnector have excellent thermal conductivities. Temperatures of the insulating layer and the interconnector are approximately equal to temperature of the photovoltaic cell. Thus, an equivalent module of the photovoltaic cell with thickness $h = H_{pv} + H_t + H_c$ is employed to represent the whole photovoltaic cell, the insulating layer and the metal interconnector, as shown in Fig. 3.

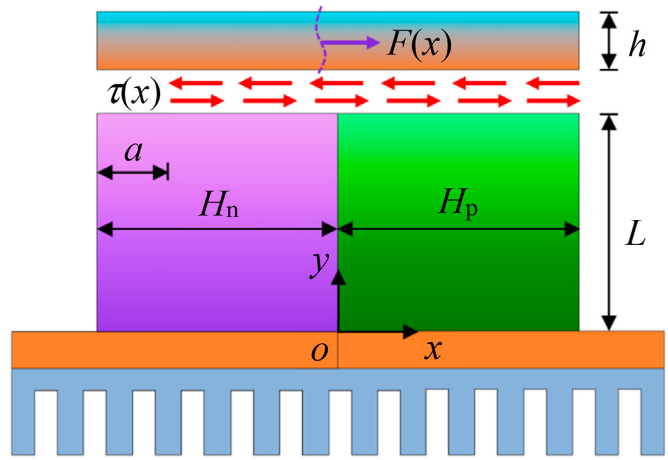

Fig. 3. The mathematical model for interlaminar stress analysis.

The mismatched axial displacements between the equivalent photovoltaic cell and the adjacent TE module resulted from the thermal stress will lead to the progressive mechanical failure of the hybrid photovoltaic-thermoelectric (PV-TE) devices. Considering the fact that the equivalent photovoltaic cell is much thinner than TE module, the hybrid device of Fig. 3 is regarded as a film (the equivalent solar cell) covering a substrate (TE module and heat sink). The interlaminar shear stress is denoted by $\tau(x)$. The axial force in the equivalent solar cell is expressed as $F(x)$. In the crack region $[-H_n, a - H_n]$, the interlaminar shear stress is zero since the crack surfaces are free.

Due to both the insulating layer and the cooper strip have great thermal conductivity and small thickness, it is assumed that temperature of the equivalent photovoltaic cell is still T_{pv}. Then, the axial strain of the equivalent photovoltaic cell reads [33,34]:

$$\varepsilon_{solar} = \alpha_{solar}\left(T_{pv} - T_0\right) - \psi F(x) \tag{13}$$

where $\psi = (1 - \upsilon_{solar})/(E_{solar}h)$ represents the coefficient of axial compliance [34], υ_{solar} denotes Poisson's ratio, α_{solar} represents the coefficient of thermal expansion and E_{soalr} is elastic modulus of the equivalent photovoltaic cell (The deriving process is given in Appendix A).

The axial strain of TE module resulted from the shear stress and the thermal loading is [35]:

$$\varepsilon_e = \frac{2}{\pi E_e} \int_{a-H_n}^{H_p} \frac{\tau(\xi)}{\xi - x} d\xi + \alpha_e (T_1 - T_0) \tag{14}$$

where α_e and E_e are the equivalent elastic modulus and the equivalent coefficient of thermal expansion of the TE module, those are presented in Appendix B.

The relationship between $\tau(x)$ and $F(x)$ holds: $F(x) = -W\int_{a-H_n}^{x} \tau(\xi)d\xi$. Taking the strain compatibility condition $\varepsilon_{solar} = \varepsilon_e$ into account, one can obtain:

$$\frac{2}{\pi E_e}\int_{a-H_n}^{H_p}\frac{\tau(\xi)}{\xi-x}d\xi-\psi W\int_{a-H_n}^{x}\tau(\xi)d\xi=\Delta\varepsilon_T \tag{15}$$

in which $\Delta\varepsilon_T = \alpha_{solar}(T_{pv} - T_0) - \alpha_e(T_1 - T_0)$.

By using the coordinate transformations $\xi = \overline{\xi}(H_n + H_p - a)/2 + (H_p + a - H_n)/2, -1<\overline{\xi}<1$ and $x = \overline{x}(H_n + H_p + a)/2 + (H_p + a - H_n)/2, -1<\overline{x}<1$, Eq. (15) can be normalized to give:

$$\frac{2}{\pi E_e}\int_{-1}^{1}\frac{\tau(\overline{\xi})}{\overline{\xi}-\overline{x}}d\overline{\xi}-\frac{\psi}{2}WH_e\int_{-1}^{\overline{x}}\tau(\overline{\xi})d\overline{\xi}=\Delta\varepsilon_T \tag{16}$$

where $H_e = H_n + H_p - a$ represents the effective thickness of the TE module. The solution of the interlaminar shear stress in Eq. (16) has been presented in Refs. [36,37], that is:

$$\tau(\overline{x})=\frac{1}{\sqrt{1-\overline{x}^2}}\sum_{m=0}^{\infty}b_m Y_m(\overline{x}), -1<\overline{x}<1 \tag{17}$$

where b_m is the unknown parameters, $Y_m(\overline{x})$ is the Chebyshev polynomials of the first kind. Considering no external mechanical loadings acting at the hybrid PV-TE device of Fig. 3, the interlaminar shear stress must hold $\int_{a-H_n}^{H_p}\tau(x)dx = 0$, this can be used to give $b_0 = 0$.

Now, applying Eq. (17) into Eq. (16) gives:

$$\frac{2}{E_e}\sum_{m=1}^{\infty}b_m\frac{\sin[(m+1)\arccos(\overline{x})]}{\sin[\arccos(\overline{x})]}+\frac{\psi}{2}WH_e\sum_{m=1}^{\infty}\frac{b_m}{m}\sin[m\arccos(\overline{x})]=\Delta\varepsilon_T \tag{18}$$

Mathematically, Eq. (18) can be solved with the collocation method. By choosing the interpolation points $\overline{x}= \cos[(2i-1)\pi/(2M)]$, $i= 1,2,3, ..., M$, Eq. (18) reduces to

$$\frac{2}{E_e}\sum_{m=1}^{M}b_m\frac{\sin\left(m\frac{2i-1}{2M}\pi\right)}{\sin\left(\frac{2i-1}{2M}\pi\right)}+\frac{\psi}{2}WH_e\sum_{m=1}^{M}\frac{b_m}{m}\sin\left(m\frac{2i-1}{2M}\pi\right)=\Delta\varepsilon_T, i=1,2,...,M \tag{19}$$

By solving Eq. (19), one can obtain the solution of the parameters b_m and expression of $\tau(x)$ is also obtained. Then, the stress intensity factors at $x = H_p$ and $x = a - H_n$ are given by Ref. [36]: $K_{right} = \lim_{x\to H_p}\sqrt{2\pi(H_p - x)}\tau(x)$ and $K_{left} = \lim_{x\to a-H_n}\sqrt{2\pi(x + H_n - a)}\tau(x)$. With the use of Eq. (17), the stress intensity factors K_{right} and K_{left} reduces to:

$$K_{right}=\sqrt{\frac{\pi H_e}{2}}\sum_{m=1}^{M}b_m, K_{left}=\sqrt{\frac{\pi H_e}{2}}\sum_{m=1}^{M}(-1)^m b_m \tag{20}$$

The fatigue crack will propagate when $K_{max} > K_s$, in which K_s is the fracture toughness of the silver paste that can be determined by fracture experiment, S_{max} represents the maximum value of K_{right} and K_{left}. The critical loading of crack propagation can be obtained by setting $K_{max} = K_s$. Under the cyclic solar radiation, the fatigue cracking behavior of the hybrid devices will be evaluated. By using the Paris law, the crack growth rate reads to Refs. [38,39]:

$$\frac{da}{dN}=C_1(\Delta K)^{C_2} \tag{21}$$

where a denotes the crack length, N is the cyclic number of solar radiation, ΔK represents the stress intensity factor range, C_1 and C_2 denote Paris' constants (C_2 is also called the Paris' index of fatigue crack growth) determined by materials. Physically, values of K_{right} and K_{left} are zero for the case of no solar radiation, this means $\Delta K = K_{max}$.

For the given solar radiance, the length of fatigue crack after N cycles and the effect of fatigue cracking on performance of the hybrid devices are evaluated with the iteration method. The computational code is developed in the mathematical programming environment Matlab. The technical route of this paper is illustrated in Fig. 4 and outlined as follows: (I) For the given initial crack length a_0 and solar radiation G, calculating temperature of the photovoltaic cell T_{pv} and temperature at the hot side of the TE module T_1 with Eqs. (3) and (10); (II) Calculating distribution of the interlaminar shear stress $\tau(x)$ with Eq. (17); (III) Determining the maximum value of K_{left} and K_{right} with Eq. (20); (IV) After one thermal cycle, calculating the new crack length a with Eq. (21) and judging whether $a < a_c$ is satisfied, in which a_c is the critical length of fatigue crack; (V) For the case of $a < a_c$, determining the total electric power $P_{PV\text{-}TE}$ and efficiency $\eta_{PV\text{-}TE}$ with Eqs. (1), (5) and (7); (VI) Repeating the above steps and updating the crack length after each thermal cycle and power output until $a > a_c$, the number of thermal cycle is considered as the fatigue life. With the above iteration method, one can evaluate the fatigue life and reveal the effect of fatigue cracking on performance of the PV-TE devices.

4. Model verification

Dimensions and material properties of the photovoltaic sell are $H_{pv} = 0.3$ mm, $k_{pv} = 148$ W/(m•K), $\lambda = 0.9$, $\eta_{ref} = 15\%$ and $\beta_{ref} = 0.004$ K^{-1} [14]. The insulating layer is simulated by Tedlar whose thickness and thermal conductivity are $H_t = 0.175$ mm and $k_t = 0.2$ W/(m•K). The metallic interconnector is modeled by the cooper strip with thickness $H_c = 0.1$ mm and thermal conductivity $k_c = 401$ W/(m•K). Then, the thermal resistances of the photovoltaic cell, insulating layer and metal interconnector are $\kappa_{pv} = 20.27 \times 10^{-5}$ (K m^2)/W, $\kappa_t = 0.875 \times 10^{-5}$ (K m^2)/W and $\kappa_c = 0.02494 \times 10^{-5}$ (K m^2)/W. The n-type TE leg has the same dimensions 4 mm × 4 mm × 4 mm as that of p-type, and their material parameters are listed in Table 1. Temperature of the TE module at the cold side is $T_0 = 298$ K. The external electrical resistance equals that of the TE module.

For the typical geometric concentration factor $C = 1, 2, 3$ and 4, distributions of efficiency of the PV-TE device are shown in Fig. 5. It is clearly seen from graph in Fig. 5 that efficiency of the hybrid device given in Ref. [14] is in good agreement with results obtained in the present study. This demonstrates the mathematical model used in the present study is available.

5. Numerical results and discussions

Based on the photovoltaic-thermoelectric (PV-TE) model verified above, the fatigue cracking behavior and its effect on energy conversion performance are analyzed subsequently. The photovoltaic module is simulated by the commercial silicon-based photovoltaic cell. In the practical applications, the electric insulation layer can be Tedlar and ceramic plate [14,27]. Here, the dense ZrO_2 ceramic plate is considered to model the electric insulation layer. The thermoelectric (TE) legs are simulated by bismuth telluride (Bi_2Te_3). The material properties of every components of the hybrid devices are listed in Table 2. In this section, dimensions of the hybrid devices used in the numerical examples are the same as those given in Section 4. The thickness ratio of the silver paste to the metal interconnector is $H_s/H_c = 0.01$.

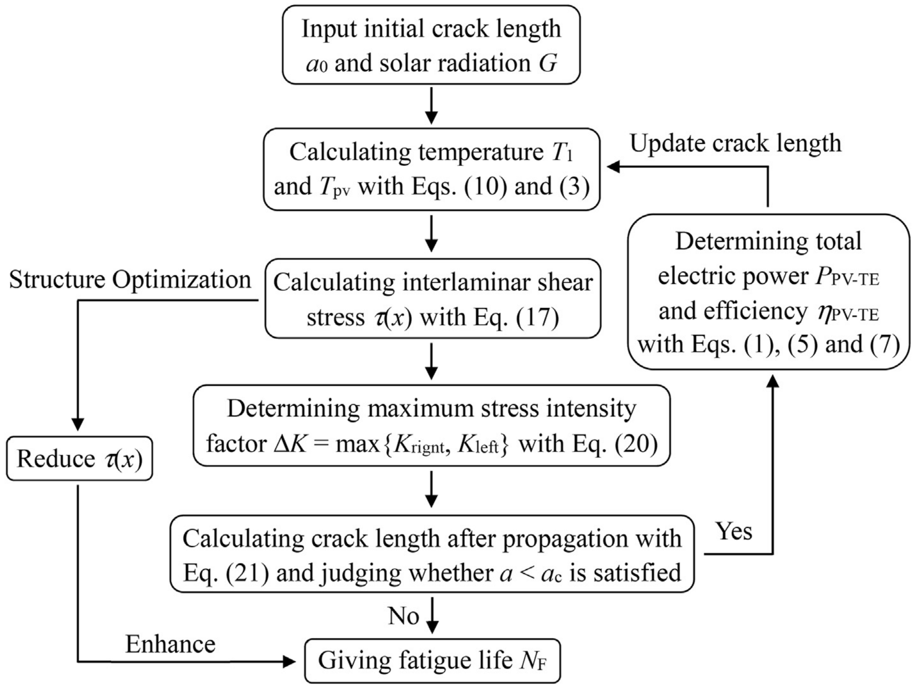

Fig. 4. Flowchart of evaluating fatigue cracking and its effect on energy conversion performance.

Table 1
Material parameters for thermoelectric legs presented in Ref. [14].

Parameter	Value	Unit
k_n	$3.3455 \times 10^{-5}T^2 - 0.02335T + 5.6063$	W/(m·K)
k_p	$3.6156 \times 10^{-5}T^2 - 0.02635T + 6.2216$	W/(m·K)
s_n	$1.5307 \times 10^{-3}T^2 - 1.0806T - 28.3381$	μV/K
s_p	$2.7438T - 3.6381 \times 10^{-3}T^2 - 296.214$	μV/K
$1/\rho_n$	$(1.0571T^2 - 10.1605T + 3113.714) \times 10^2$	Ω·m
$1/\rho_p$	$(1.5602T\text{-}15.7081 \times 10^{-3}T^2\text{-}4466.381) \times 10^6$	Ω·m

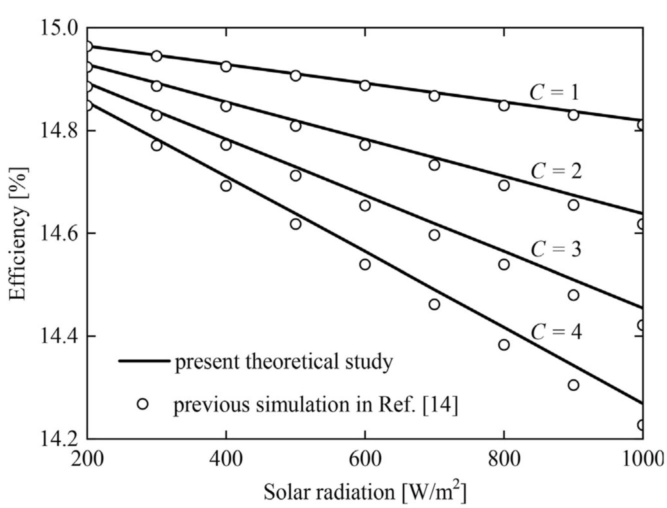

Fig. 5. Efficiency validation of previous simulation with present study.

5.1. Fatigue crack growth and lifetime evaluation

It was reported that the Paris' constants were $C_1 = 4.9 \times 10^{-20}$ and $C_2 = 2$ for a cooper strip bonded to the bismuth telluride TE module [44]. Fig. 6 presents the normalized crack length with respect to the cyclic number. It is found that the fatigue crack growth can be divided into three stages. Firstly, the micro-crack slowly propagates and nucleates into a macroscopic crack with the cyclic solar radiance. With the further propagation of crack, the equivalent photovoltaic cell gradually delaminates from the TE module. Physically, the crack hinders heat transferring from the equivalent photovoltaic cell into TE module, this certainly introduces a larger value of $T_{pv} - T_1$ (a larger interlaminar thermal stress) between the two adjacent modules. As a result, crack growth rate increases with the crack length in this stage. In the third stage, the equivalent photovoltaic cell finally delaminates from the TE module and the hybrid PV-TE system surfers the fatigue failure.

As illustrated in Fig. 4, the energy conversion performance and lifetime of the hybrid devices are closely related to the crack length. However, the crack length derived from Eq. (21) is an extremely complex expression with respect to the cyclic number. There is a real need to present a simple but useful expression of the fatigue crack length to guide the engineering applications. Based on the data shown in Fig. 6 and the data analysis software OriginPro 2021b (Learning Edition), the crack length can be fitted as follows:

$$\frac{a}{H_n} = m_1 + \frac{m_2}{N + m_3} \tag{22}$$

where N represents the cyclic number, m_1, m_2 and m_3 are parameters related to material properties and can be determined by experiments. For the typical $C = 80$, the parameters shown in Eq. (22) are determined as $m_1 = 0.9847$, $m_2 = -587327$ and $m_3 = 598919$. It is found that the fitting expression agrees well with the analytical solution. For the critical crack length $a_c/H_n = 0.97$, the fatigue life derived from Eq. (22) is about $N_F = 3.93 \times 10^7$. Additionally, the analytical fatigue life is about $N_F = 3.62 \times 10^7$. The error of fatigue life between analytical solution and the fitting expression is 7.9%. In a word, the fitting crack length with respect to cyclic number shown in Eq. (22) is useful and can be accepted in the engineering applications.

Table 2
Material properties of each component in the hybrid PV-TE device.

Parameters	Value	References	Parameters	Value	References
λ	0.9	[14]	υ_t	0.333	[41]
η_{ref}	15%	[14]	α_t [K^{-1}]	8.78×10^{-6}	[41]
β_{ref} [K^{-1}]	0.004	[14]	k_c [W/(m·K)]	300	[42]
k_{pv} [W/(m·K)]	148	[14]	E_c [GPa]	119	[42]
E_{pv} [GPa]	130	[40]	υ_c	0.326	[42]
υ_{pv}	0.28	[40]	α_c [K^{-1}]	17.7×10^{-6}	[42]
α_{pv} [K^{-1}]	2.92×10^{-6}	[40]	ρ_c [Ω·m]	2.5×10^{-8}	[42]
k_t [W/(m·K)]	1.78	[41]	k_s [W/(m·K)]	420	–
E_t [GPa]	114	[41]	ρ_s [Ω·m]	1.65×10^{-8}	–

Parameters	Value	References
k_n [W/(m·K)]	$-6.943 \times 10^{-6}T^2 + 5.41 \times 10^{-3}T + 0.2008$	[43]
k_p [W/(m·K)]	$-1.294 \times 10^{-5}T^2 + 1.037 \times 10^{-2}T - 0.8501$	[43]
ρ_n [μΩ·m]	$8.068 \times 10^{-5}T^2 - 3.61 \times 10^{-2}T + 13.74$	[43]
ρ_p [μΩ·m]	$-4.666 \times 10^{-5}T^2 + 9.326 \times 10^{-2}T - 14.37$	[43]
s_n [μV/K]	$1.174 \times 10^{-3}T^2 - 1.078T + 57.8$	[43]
s_p [μV/K]	$-3.202 \times 10^{-3}T^2 + 2.504T - 269.1$	[43]
α_n (α_p) [10^{-5}/K]	$-3.619 \times 10^{14}T^{-6.03} + 1.316$	[43]
E_n (E_p) [GPa]	$-0.015T + 67.8$	[43]
υ_n (υ_p)	0.23	[43]

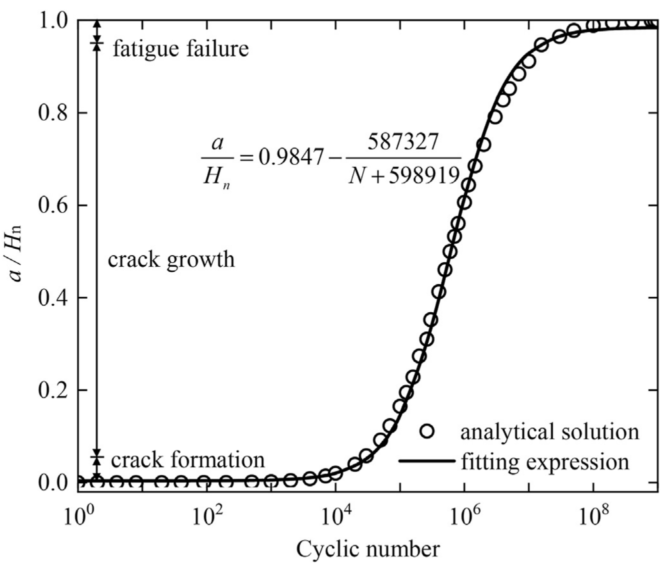

Fig. 6. The normalized crack length with respect to the cyclic number (C = 80, η_{ref} = 15% and β_{ref} = 0.004 K^{-1}).

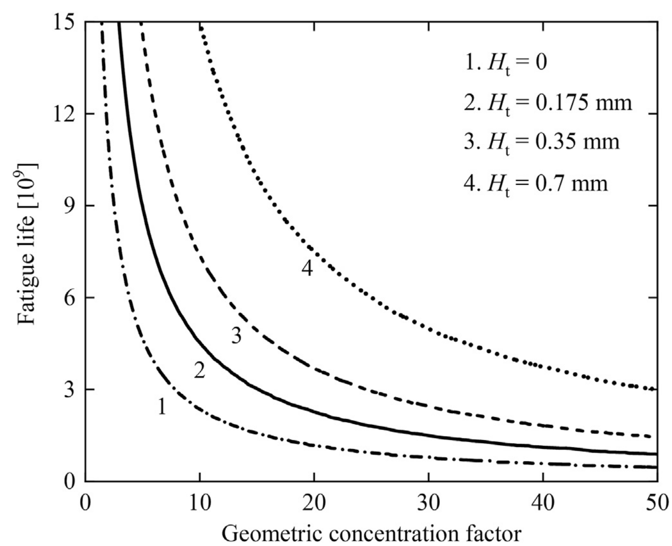

Fig. 7. Effect of electric insulation layer's thickness on lifetime (η_{ref} = 15%, β_{ref} = 0.004 K^{-1}).

For different values of H_t, Fig. 7 gives the fatigue life as a function of the geometric concentration factor. Clearly, the fatigue life is gradually reduced with the geometry concentration factor. This is caused by the fact that a bigger value of C causes a higher thermal stress in the hybrid devices. It is also found that lifetime of the hybrid devices increases with the insulating layer's thickness. Physically, a thicker insulating layer means a larger thermal resistance between the photovoltaic cell and the TE module. Considering the value of $\kappa_t = H_t/k_t$ is very small in the actual applications, the increase of κ_t has very small influence on temperature of the hybrid devices. In this regard, effect of variation of H_t on the lifetime of the hybrid devices should be ignored. However, variation of H_t will simultaneously change the equivalent mechanical properties of the photovoltaic cell as shown in Eq. (A5). Considering the fact that $H_t < H_{pv}$ and $\alpha_t > \alpha_{pv}$, value of α_{solar} certainly increases with h_t. This will reduce the difference between α_{solar} and α_e. This means a decrease of the relative displacement between the equivalent photovoltaic cell and the TE module. This indicates that $\tau(x)$ in the hybrid devices decreases with H_t. As a result, the lifetime of the hybrid devices increases with H_t.

5.2. Effect of fatigue cracking on energy conversion performance

The crack hinders the heat conducting from photovoltaic cells into thermoelectric module, this certainly affects performance of the hybrid devices. For different types of the photovoltaic cells, the electric powers generated by the hybrid devices versus the crack length are presented in Fig. 8. The normalized crack length $a/H_n = 1$ denotes the TE module completely delaminates from the photovoltaic cell, and the photovoltaic cell works alone for this case.

For the photovoltaic cells with a small temperature coefficient (e.g. β_{ref} = 0.001 K^{-1}), the electric power of the hybrid devices is much bigger than that of the photovoltaic cell works alone. For instance, electric power of the photovoltaic cell (β_{ref} = 0.001 K^{-1} and η_{ref} = 10%) works alone and the hybrid device are 230.6 mW and 248.6 mW. Inclusion of thermoelectric module with a photovoltaic cell improves the electric power by 7.8%. This means

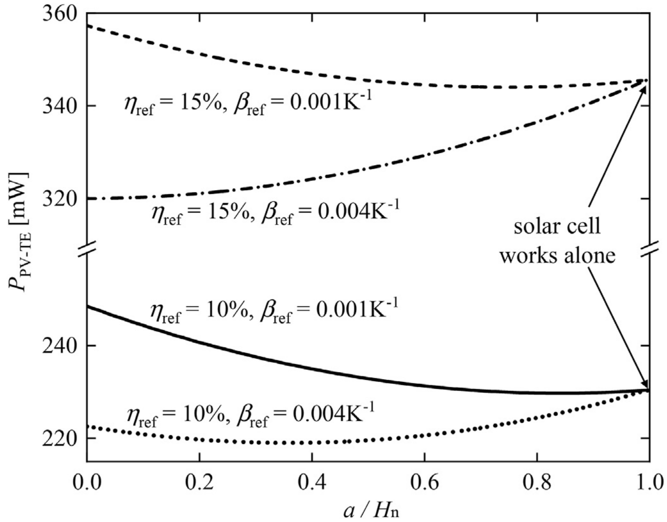

Fig. 8. Power output of the hybrid devices versus crack length (C = 80).

photovoltaic cell with a small temperature coefficient is suitable for combining with thermoelectric module to enhance total electric power. With propagation of the fatigue crack, the electric power of the hybrid devices gradually decreases to the same value as that of the photovoltaic cell works alone. Physically, the crack growth enlarges the electrical and electrical contact resistances of the hybrid devices. This weakens the heat transferring from the photovoltaic cell into the TE module. As a result, value of T_1 is decreased thus leads to P_{TE} significantly reduced. This causes the total power output decrease of the hybrid devices. For the photovoltaic cells with a large temperature coefficient (e.g. $\beta_{ref} = 0.004$ K^{-1}), the electric power of the hybrid devices is much smaller than that of the photovoltaic cell works alone. For instance, electric power of the photovoltaic cell ($\beta_{ref} = 0.004$ K^{-1} and $\eta_{ref} = 10\%$) works alone and the hybrid device are 230.6 mW and 223 mW. Inclusion of thermoelectric module with a photovoltaic cell reduces the electric power by 3.3%. This means the photovoltaic cells with a large temperature coefficient is not appropriate for combining the hybrid PV-TE devices. Additionally, it is found that the electric power of the hybrid devices firstly decreases then climbs to a peak value with crack length when the photovoltaic cells have a small reference efficiency and a large temperature coefficient (e.g. $\eta_{ref} = 10\%$ and $\beta_{ref} = 0.004$ K^{-1}). As described above, the crack growth will lower the temperature of the hybrid system, this simultaneously results in P_{TE} decreasing and P_{pv} increasing. For the small crack length, the value decrease of P_{TE} is bigger than increase of P_{pv}. As a result, value of $P_{\text{PV-TE}}$ decreases with crack length. With the crack further propagation, improvement of P_{pv} plays the chief role and leads to the increase of the electric power.

Measuring the crack length at the interface between the metal interconnector and the TE module is extremely hard. Thus, the direct evaluation of total electric power of the hybrid devices versus crack length is inconvenient and unreasonable in the engineering applications. The electric power with respect to the cyclic number is given in Fig. 9. It is found that value of $P_{\text{PV-TE}}$ is inversely proportional to value of N. The fitting expression of power output is well agreement with that of the analytical solution. This means the fitting power output with respect to cyclic number is useful and can be accepted in the engineering applications. Since the crack length is barely changed when the cyclic number is relative small (e.g. $N < 10^4$), the power output keeps a constant for this case. With the further increase of the cyclic number, the crack sharply propagates.

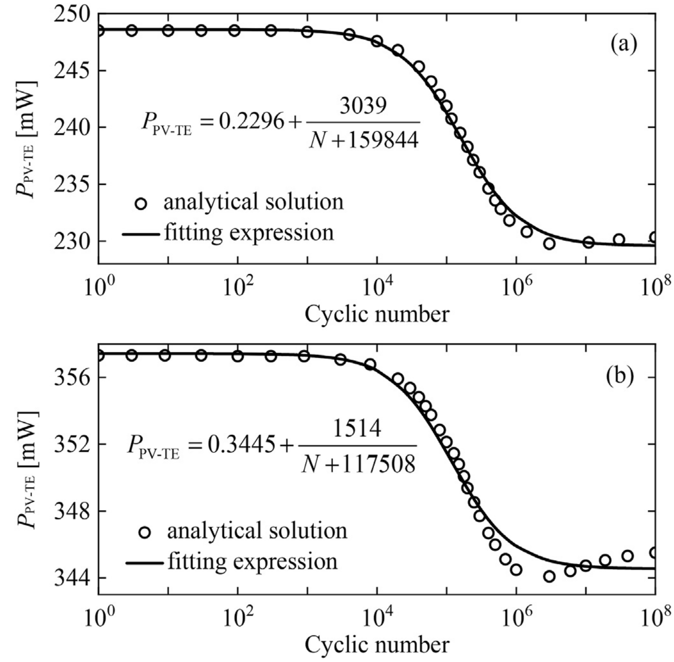

Fig. 9. Power output of the hybrid devices for photovoltaic cell with (a) $\eta_{ref} = 10\%$, $\beta_{ref} = 0.001$ K^{-1} and (b) $\eta_{ref} = 15\%$, $\beta_{ref} = 0.001$ K^{-1}..

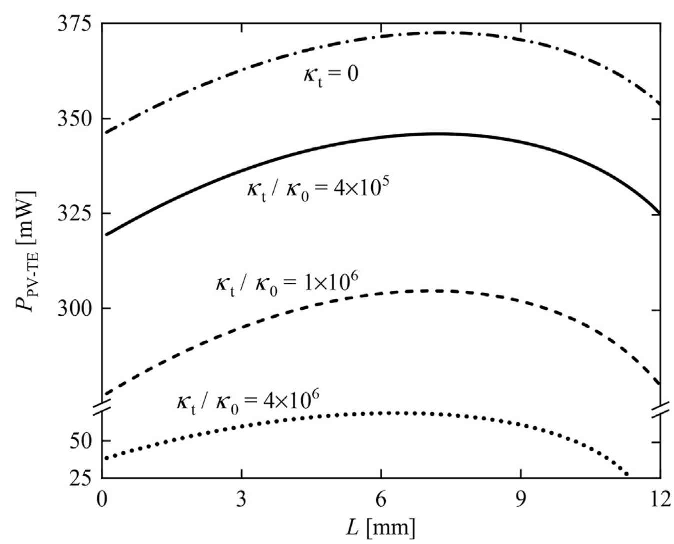

Fig. 10. Distribution of power output versus of length of TE module without considering crack ($\eta_{ref} = 15\%$ and $\beta_{ref} = 0.001$ K^{-1}).

This results in a decrease of the electric power. The electric power output of the hybrid devices is inversely proportional to the cyclic number.

5.3. Optimization of hybrid PV-TE devices

For different values of κ_t, Fig. 10 gives the electric power without considering the fatigue crack, in which $\kappa_0 = 9.83 \times 10^{-5}$ (K m^2)/W. Clearly, a larger thermal resistance results in a smaller electric power of the hybrid devices. Physically, the heat flux becomes harder to transfer from the photovoltaic cells into the (thermoelectric) TE module when the hybrid devices have a bigger thermal resistance. This means value of $T_1 - T_0$ decreasing and T_{pv}

increasing with the thermal resistance. Based on the Seebeck coefficient, a lower value of $T_1 - T_0$ means a smaller power output generated by the TE module [45,46]. Additionally, Eqs. (1) and (2) indicate that value of P_{pv} gradually decreases with the working temperature. This means the photovoltaic cells will lose the ability of converting solar energy into electricity when its temperature is high enough. As a result, the electric power of the hybrid device decreases with the thermal resistance.

It is also found that $P_{PV\text{-}TE}$ firstly climbs to the maximum value and then slides with L. Physically, the length increase of the TE module simultaneously introduces a higher temperature of the hybrid devices and a bigger electrical resistance. For the small value of L, improvement of $T_1 - T_0$ plays the leading role. Thus, the total electric power of the hybrid devices gradually climbs to the peak value. With the further increase of length, the temperature increase of the hybrid devices oppositely reduces the value of P_{pv}. Additionally, the Journal heat also increases with the electric resistance. Resultant of these two effects results in a decrease of $P_{PV\text{-}TE}$. Overall, value of L can be optimized to get the maximum value of $P_{PV\text{-}TE}$.

For the given materials and configuration of the PV-TE devices, coefficient of thermal expansion of the equivalent photovoltaic cell is $\alpha_{solar} = 7.053 \times 10^{-6}\ \mathrm{K}^{-1}$ by using Eq. (A2) in Appendix A. For the different values $\alpha_e/\alpha_{solar} = 0.5$, 1 and 2, Fig. 11 presents the distribution of interlaminar shear stress without considering fatigue crack. It is clearly seen from the paragraph that sign of $\tau(x)$ for $\alpha_e/\alpha_{solar} = 0.5$ is opposite to that for $\alpha_e/\alpha_{solar} = 2$. Physically, elongation induced by free expansion of the TE module is smaller than that of the equivalent photovoltaic cell for $\alpha_e/\alpha_{solar} = 0.5$. This means the TE module inhibiting elongation of the equivalent photovoltaic cell. Therefore, the actual $\tau(x)$ in the equivalent photovoltaic cell is along the positive direction of x-axis in the region $-H_n < x < 0$, and along the opposite direction in the region $0 < x < H_p$. Similarly, the TE module elongates the equivalent photovoltaic cell for $\alpha_e/\alpha_{solar} = 2$. For this case, the actual $\tau(x)$ of the equivalent photovoltaic cell is opposite to that for $\alpha_e/\alpha_{solar} = 0.5$. Most importantly, it is noted that $\tau(x)$ is approximately vanished if $\alpha_e = \alpha_{solar}$. This means $\tau(x)$ in the hybrid devices can be reduced by optimizing the value of α_e and α_{solar}. Under the hypothesis that $a_{ne} = a_{pe}$, Eq. (B4) presented in Appendix B clearly shows that $a_e = a_{ne}$. This means value of a_e is independent of dimensions of the TE module. Therefore, thickness of the photovoltaic module will be optimized to reduce the interlaminar shear stress. By setting $\alpha_{solar} = \alpha_e$ and using Eq. (A2) presented in Appendix A, one can obtain:

$$\frac{H_{pv}}{H_t} = \frac{(\alpha_t - \alpha_{ne})E_t}{(\alpha_{ne} - \alpha_{pv})E_{pv}} + \chi \frac{(\alpha_c - \alpha_{ne})E_c}{(\alpha_{ne} - \alpha_{pv})E_{pv}} \tag{23}$$

in which, χ denotes the thickness ratio of the metal interconnector to the insulating layer.

As shown in Eq. (23) that the thickness ratio H_{pv}/H_t is a function with respect to α_{ne} and α_{pe}. In practical applications, values of α_{ne} and α_{pe} are verified with the concentrated solar irradiance. To vanish the interlaminar shear stress in the hybrid devices, thickness ratio of the photovoltaic module to the insulating layer can be optimized for different solar irradiances.

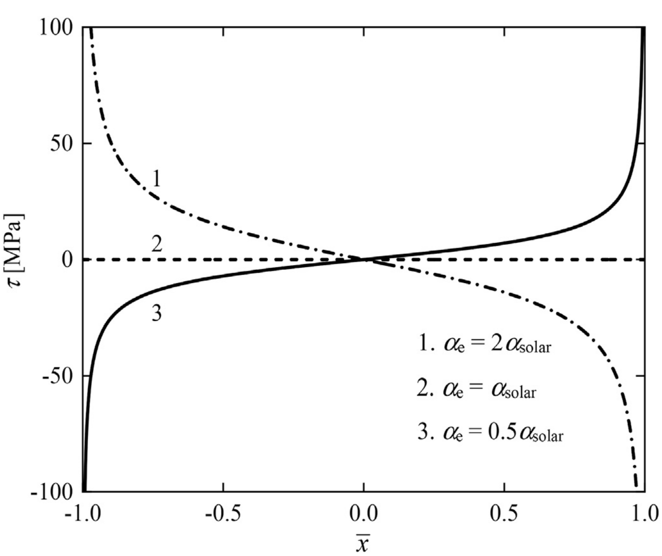

Fig. 11. The interlaminar shear stress for different coefficients of thermal expansion($C = 80$).

6. Conclusions

Crack propagation and its effect on the electric power of a photovoltaic-thermoelectric (PV-TE) devices subjected to the cyclic solar irradiance are analyzed. The thermoelectric (TE) module is behind the photovoltaic (PV) cell sandwiched by an insulating layer. For the PV cell with temperature coefficient $\beta_{ref} = 0.001\ \mathrm{K}^{-1}$, results show that combining TE model with PV cell can improve electric power by 7.8%. On the other hand, the total electric power reduces by 3.3% when temperature coefficient is $\beta_{ref} = 0.004\ \mathrm{K}^{-1}$. The total electric power of the PV-TE devices climbs to the maximum value and then slides with the length of the TE module. With the propagation of fatigue crack, the total electric power decreases when the PV cell with a small temperature coefficient (e.g. $\beta_{ref} = 0.001\ \mathrm{K}^{-1}$) but increases when the PV cell with a large temperature coefficient (e.g. $\beta_{ref} = 0.004\ \mathrm{K}^{-1}$). A simplified yet useful expression for power output prediction versus the cyclic number of solar irradiance is given. It is found that the electric power is inversely proportional to the cyclic number. By regulating the thickness ratio of the photovoltaic cell to the insulating layer as shown in Eq. (24), the interlaminar shear stress in the PV-TE devices can be eliminated thus the fatigue life of the hybrid devices is greatly improved.

CRediT authorship contribution statement

Y.J. Cui: Methodology, Formal analysis, Writing – original draft, Software. **B.L. Wang:** Conceptualization, Writing – review & editing, Funding acquisition. **K.F. Wang:** Writing – review & editing, Funding acquisition. **G.G. Wang:** Writing – original draft, Writing – review & editing. **A.B. Zhang:** Writing – review & editing, Software.

Declaration of competing interest

The authors declare that they have no known competing financial interests or personal relationships that could have appeared to influence the work reported in this paper.

Acknowledgements

This research was supported by the National Natural Science Foundation of China (project nos. 11972137, 11972133 and 12102104) and Guangdong Basic and Applied Basic Research Foundation (Project No. 2019A1515011348).

Appendix A. Equivalent material properties of the photovoltaic cell

For the photovoltaic cells subjected to a thermal load ΔT, the thermally induced axial strain is: $\varepsilon_{pv\text{-}T} = \alpha_{pv}\Delta T + F_{pv}/(E_{pv}H_{pv}W)$, in which α_{pv} is coefficient of thermal expansion, E_{pv} is elastic modulus, F_{pv} is the axial thermal force in the photovoltaic cell. Similarly, the axial strain of the insulating layer and metal interconnector can be respectively written as: $\varepsilon_{t\text{-}T} = \alpha_t\Delta T + F_t/(E_tH_tW)$ and $\varepsilon_{c\text{-}T} = \alpha_c\Delta T + F_c/(E_cH_cW)$, where α_t is coefficient of thermal expansion, E_t is elastic modulus and F_t is axial thermal stress of the insulating layer; α_c, E_c and F_c are coefficient of thermal expansion, elastic modulus and axial thermal stress of the metal interconnector. Additionally, the force balance condition in axial direction indicates: $F_{pv} + F_t + F_c = 0$. Based on the compatibility condition of deformation, relationship among $\varepsilon_{pv\text{-}T}$, $\varepsilon_{t\text{-}T}$ and $\varepsilon_{c\text{-}T}$ must hold: $\varepsilon_{pv\text{-}T}(H_n+H_p) = \varepsilon_{t\text{-}T}(H_n+H_p) = \varepsilon_{c\text{-}T}(H_n+H_p)$, this can be used with the force balance condition to give:

$$\frac{F_t}{E_tH_tW} = \frac{E_cH_c(\alpha_c-\alpha_t) - E_{pv}H_{pv}(\alpha_t-\alpha_{pv})}{E_{pv}H_{pv}+E_tH_t+E_cH_c}\Delta T \tag{A1}$$

For the equivalent photovoltaic cell subjected to the thermal load ΔT, the axial strain can be directly expressed as $\varepsilon_{solar\text{-}T} = \alpha_{solar}\Delta T$. By setting $\varepsilon_{solar\text{-}T} = \varepsilon_{t\text{-}T}$, one can obtain:

$$\alpha_{solar} = \frac{E_{pv}H_{pv}\alpha_{pv}+E_tH_t\alpha_t+E_cH_c\alpha_c}{E_{pv}H_{pv}+E_tH_t+E_cH_c} \tag{A2}$$

For the equivalent photovoltaic cell subjected to the external axial force ΔF along the x-direction, the axial strain of the photovoltaic cell, the insulating layer and the metal interconnector are: $\varepsilon_{pv\text{-}T} = F_{pv}/(E_{pv}H_{pv}W)$, $\varepsilon_{t\text{-}T} = F_t/(E_tH_tW)$ and $\varepsilon_{c\text{-}T} = F_c/(E_cH_cW)$, in which F_{pv}, F_t and F_c are axial force components in the photovoltaic cell, the insulating layer and the metal interconnector. The force balance condition indicates the axial force components must hold the following relationship: $F_{pv} + F_t + F_c = \Delta F$. Then, the compatibility condition of deformation $\varepsilon_{pv\text{-}F}(H_n+H_p) = \varepsilon_{t\text{-}F}(H_n+H_p) = \varepsilon_{c\text{-}F}(H_n+H_p)$ can be used with the force balance condition to give:

$$F_t = \frac{E_tH_t}{E_{pv}H_{pv}+E_tH_t+E_cH_c}\Delta F, F_{pv} = \frac{E_{pv}H_{pv}}{E_tH_t}F_t, F_c = \frac{E_cH_c}{E_tH_t}F_t \tag{A3}$$

according to Hooke's law, the total deformations of the photovoltaic cell, the insulating layer and the metal interconnector along the y-direction is: $u_y = \upsilon_{pv}\varepsilon_{pv-F}H_{pv} + \upsilon_t\varepsilon_{t-F}H_t + \upsilon_c\varepsilon_{c-F}H_c$, in which υ_{pv}, υ_t and υ_c are Poisson's ratio of the photovoltaic cell, the insulating layer and the interconnector. With the use of Eq. (A3), the total deformation u_y in y-direction can be rewritten as:

$$u_y = \frac{\upsilon_{pv}H_{pv}+\upsilon_tH_t+\upsilon_cH_c}{E_{pv}H_{pv}+E_tH_t+E_cH_c}\frac{\Delta F}{W} \tag{A4}$$

For the equivalent photovoltaic cell subjected ΔF along x-direction, the axial strain in x-direction and the lateral deformation along x-direction are: $\varepsilon_{solar\text{-}F} = \Delta F/(E_{solar}hW)$ and $u_{solar\text{-}y} = \upsilon_{solar}\Delta F/(E_{solar}W)$, in which $h = H_{pv}+H_t+H_c$ represents the total thickness of the equivalent photovoltaic cell. Now, by setting $\varepsilon_{t\text{-}F} = \varepsilon_{solar\text{-}F}$ and $u_y = u_{solar\text{-}F}$, one can obtain the elastic modulus and the Poisson's ration of the equivalent photovoltaic cell, those are:

$$E_{solar} = \frac{1}{h}(E_{pv}H_{pv}+E_tH_t+E_cH_c) \tag{A5}$$

$$\upsilon_{solar} = \frac{1}{h}(\upsilon_{pv}H_{pv}+\upsilon_tH_t+\upsilon_cH_c) \tag{A6}$$

Appendix B. Equivalent material properties of the TE module

According to the generalized Hooke law, the strain of an elastic and isotropic material subjected to a normal stress σ is $\varepsilon = (1-\upsilon^2)\sigma/E$. For the thermoelectric (TE) module of Fig. 3 subjected to the longitudinal stress σ, elongation of the TE module along x-direction is:

$$u_\sigma = \frac{\sigma}{E_{ne}}\left(1-\upsilon_n^2\right)H_n + \frac{\sigma}{E_{pe}}\left(1-\upsilon_p^2\right)H_p \tag{B1}$$

where υ_n and υ_p are Poisson's ratio, E_{ne} and E_{pe} are equivalent elastic modulus of TE legs defined as [29]: $E_{ie} = \int_{T_0}^{T_1} E_i dT/\Delta T$, (i='n','p'), in which $\Delta T = T_1 - T_0$, T_1 and T_0 are temperature at $y = L$ and $y = 0$, E_n and E_p are temperature-dependent elastic modulus.

The elongation of an equivalent TE module caused by the longitudinal stress σ is $u_{\sigma e} = \sigma(H_n+H_p)/E_e$. By setting $u_\sigma = u_{\sigma e}$, one can obtain:

$$E_e = \frac{E_{ne}E_{pe}(H_n+H_p)}{(1-\upsilon_n^2)H_nE_{pe} + \left(1-\upsilon_p^2\right)H_pE_{ne}} \tag{B2}$$

The total elongation of the TE module subjected to thermal load ΔT is:

$$u_T = \alpha_{ne}\Delta TH_n + \alpha_{pe}\Delta TH_p \tag{B3}$$

where α_{ne} and α_{pe} are equivalent coefficient of thermal expansion defined as [29]: $\alpha_{ie} = \int_{T_0}^{T_1} \alpha_i dT/\Delta T$, (i='n','p'), in which α_n and α_p are functions of versus working temperature.

Deformation of the equivalent TE module caused by the thermal load ΔT can be directly written as $u_{Te} = \alpha_e\Delta T(H_n+H_p)$. Then, the equivalent coefficient of thermal expansion of TE module can be expressed as:

$$\alpha_e = \frac{\alpha_{ne}H_n+\alpha_{pe}H_p}{H_n+H_p} \tag{B4}$$

References

[1] A. Haeb, Energy harvesting: state-of-the-art, Renew. Energy 36 (2021) 2641–2654.
[2] T.M. Brugo, E. Maccaferri, D. Cocchi, et al., Self-sensing hybrid composite laminate by piezoelectric nanofibers interleaving, Compos. B Eng. 212 (2021) 108673.
[3] Q. Zhao, X.R. Guo, H.C. Zhang, et al., Performance evaluation of a novel photovoltaic-electrochemic hybrid system, Energy Convers. Manag. 195 (2019) 1227–1237.
[4] M. Thirugnanasambandam, S. Iniyan, R. Goic, A review of solar thermal technologies, Renew. Sustain. Energy Rev. 14 (2010) 312–322.
[5] M.K. Sahoo, P. Kale, Restructured porous silicon for solar photovoltaic: a review, Microporous Mesoporous Mater. 289 (2019) 109619.
[6] H.K. Lakeh, R. Hosseini, H. Kaatuzian, Numerical and experimental investigation on a thermo-photovoltaic module for higher efficiency energy generation, Int. J. Thermophys. 38 (2017) 78.
[7] A.B. Zhang, B.L. Wang, D.D. Pang, et al., Effects of interface layers on the performance of annular thermoelectric generators, Energy 147 (2018) 612–620.
[8] P.A. Cotfas, D.T. Cotfas, Comprehensive review of methods and instruments for photovoltaic-thermoelectric generator hybrid system characterization, Energies 13 (2020) 6045.
[9] H.B. Guo, G.H. Huang, H.J. Li, et al., Development of stove-powered thermoelectric generators: a review, Appl. Therm. Eng. 96 (2016) 297–310.
[10] P. Motiei, M. Yaghoubi, E. Goshtashbirad, et al., Two-dimensional unsteady state performance analysis of a hybrid photovoltaic-thermoelectric generator, Renew. Energy 119 (2018) 551–565.
[11] J. Zhang, Y.M. Xuan, L.L. Yang, Performance estimation of photovoltaic-thermoelectric hybrid systems, Energy 78 (2014) 895–903.
[12] E. Yin, Q. Li, Y.M. Xuan, Thermal resistance analysis and optimization of photovoltaic thermoelectric hybrid system, Energy Convers. Manag. 143 (2017) 188–202.
[13] A. Rezania, L.A. Rosendahl, Feasibility and parametric evaluation of hybrid concentrated photovoltaic-thermoelectric system, Appl. Energy 187 (2017) 380–389.
[14] G.Q. Li, S. Shittu, X.L. Ma, et al., Comparative analysis of thermoelectric

elements optimum geometry between photovoltaic-thermoelectric and solar thermoelectric, Energy 171 (2019) 599–610.
[15] E. Yin, Q. Li, Y.M. Xuan, Optimal design method for concentrating photovoltaic-thermoelectric hybrid system, Appl. Energy 226 (2018) 320–329.
[16] S. Shittu, G.Q. Li, X.D. Zhao, Comparative study of a concentrated photovoltaic-thermoelectric system with and without flat plate heat pipe, Energy Convers. Manag. 193 (2019) 1–14.
[17] A. Abdo, T. Saito, S. Ookawara, et al., Experimental study of the performance of a concentrator photovoltaic/thermoelectric generator system integrated with a new 3D printed microchannel heat sink, Int. J. Energy Res. 45 (2021) 7741–7763.
[18] J. Zhang, H. Zhai, Z.H. Wu, et al., Enhanced performance of photovoltaic-thermoelectric coupling devices with thermal interface materials, Energy Rep. 6 (2020) 116–122.
[19] E. Yin, Q. Li, Y.M. Xuan, Feasibility analysis of a tandem photovoltaic-thermoelectric hybrid system under solar concentration, Renew. Energy 162 (2020) 1828–1841.
[20] K.G. Ismaila, A.Z. Sahin, B.S. Yilbas, Exergo-economic optimization of concentrated solar photovoltaic and thermoelectric hybrid generator, J. Therm. Anal. Calorim. (2021), https://doi.org/10.1007/s10973-020-10508-1.
[21] H.P. Song, K.K. Xie, C.F. Gao, Progressive thermal stress distribution around a crack under Joule heating in orthotropic materials, Appl. Math. Model. 86 (2020) 271–293.
[22] B.L. Wang, Y.J. Cui, Transient interlaminar thermal stress in multi-layered thermoelectric materials, Appl. Therm. Eng. 119 (2017) 207–214.
[23] E. Hatzikraniotic, K.T. Zorbas, I. Samaras, et al., Efficiency study of a commercial thermoelectric power generator (TEG) under thermal cycling, J. Electron. Mater. 39 (2010) 2112–2116.
[24] M.T. Barako, W. Park, A.M. Marconnet, et al., Thermal cycling, mechanical degradation, and the effective figure of merit of a thermoelectric module, J. Electron. Mater. 42 (2013) 372–381.
[25] W. Park, M.T. Barako, A. Marconnet, et al., Effect of thermal cycling on commercial thermoelectric modules, Intersociety conference on thermal and thermomechanical phenomena in electronic systems 16 (2012) 107–112.
[26] Y.J. Cui, B.L. Wang, J.E. Li, et al., Performance evaluation and lifetime prediction of a segmented photovoltaic-thermoelectric hybrid system, Energy Convers. Manag. 211 (2020) 112744.
[27] P.M. Rodrigoa, A. Valera, E.F. Fernández, et al., Performance and economic limits of passively cooled hybrid thermoelectric generator-concentrator photovoltaic modules, Appl. Energy 238 (2019) 1150–1162.
[28] Y.J. Cui, B.L. Wang, K.F. Wang, Energy conversion performance optimization and strength evaluation of a wearable thermoelectric generator made of a thermoelectric layer on a flexible substrate, Energy 229 (2021) 120694.
[29] E. Kanimba, Z.T. Tian, A new dimensionless number for thermoelectric generator performance, Appl. Therm. Eng. 152 (2019) 858–864.
[30] M. Gomez, R. Reid, B. Ohara, et al., Influence of electrical current variance and thermal resistances on optimum working conditions and geometry for thermoelectric energy harvesting, J. Appl. Phys. 113 (2013) 174908.
[31] Y.J. Cui, B.L. Wang, K.F. Wang, et al., Power output evaluation of a porous annular thermoelectric generator for waste heat harvesting, Int. J. Heat Mass Tran. 137 (2019) 979–989.
[32] Y.J. Cui, K.F. Wang, J.E. Li, et al., Time-dependent power output and elastic/plastic fracture analyses of porous thermoelectric ceramics for generators, Ceram. Int. 46 (2020) 8264–8273.
[33] E. Suhir, An approximate analysis of stresses in multilayered elastic thin films, J. Appl. Mech. 55 (1988) 143–148.
[34] Y.J. Cui, B.L. Wang, P. Wang, Analysis of thermally induced delamination and buckling of thin-film thermoelectric generators made up of pn-junctions, Int. J. Mech. Sci. 149 (2018) 393–401.
[35] N.I. Muskhelishvili, Some Basic Problems of the Mathematical Theory of Elasticity, Noordhoff, Groningen, 1953, pp. 391–413.
[36] Y.T. Zhou, X.J. Tian, F.J. Li, On coupling contact analysis of thermoelectric materials, Appl. Math. Model. 89 (2021) 1459–1474.
[37] Y.J. Cui, B.L. Wang, L. Zheng, et al., Theoretical model of fatigue crack growth of a thermoelectric pn-junction bonded to an elastic substrate, Mech. Mater. 151 (2020) 103623.
[38] A. Carpinteri, N. Pugno, Thermal loading in multi-layered and/or functionally graded materials: residual stress field, delamination, fatigue and related size effects, Int. J. Solid Struct. 43 (2006) 828–841.
[39] W.F. Hu, W.Y. Chen, X.B. Wang, et al., A computational framework for coating fatigue analysis of wind turbine blades due to rain erosion, Renew. Energy 170 (2021) 236–250.
[40] S.K. Tippabhotla, N.G. Diesta, X.G. Zhang, et al., Thermomechanical residual stress evaluation in multi-crystalline silicon solar cells of photovoltaic modules with different encapsulation polymers using synchrotron X-ray micro-diffraction, Sol. Energy Mater. Sol. Cell. 193 (2019) 387–402.
[41] Z. Li, B.L. Wang, K.F. Wang, et al., A multi-scale model for predicting the thermal shock resistance of porous ceramics with temperature-dependent material properties, J. Eur. Ceram. Soc. 39 (2019) 2720–2730.
[42] Y.J. Wu, T.Z. Ming, X.H. Li, et al., Numerical simulations on the temperature gradient and thermal stress of a thermoelectric power generator, Energy Convers. Manag. 88 (2014) 915–927.
[43] Y.J. Cui, K.F. Wang, B.L. Wang, et al., A comprehensive analysis of delamination and thermoelectric performance of thermoelectric pn-junctions with temperature-dependent material properties, Compos. Struct. 229 (2019) 111484.
[44] P. Wang, J.E. Li, B.L. Wang, et al., Lifetime prediction of thermoelectric devices under thermal cycling, J. Power Sources 437 (2019) 226861.
[45] S.F. Fan, Y.W. Gao, A. Rezania, Thermoelectric performance and stress analysis on wearable thermoelectric generator under bending load, Renew. Energy 173 (2021) 581–595.
[46] Q.N. Liu, S.H. Ding, Field intensity factors of three cracks originating from a circular hole in a thermoelectric material, J. Mech. Mater. Struct. 15 (2020) 605–617.